AGU ADVANCING EARTH AND SPACE SCIENCES

Water Resources Research

RESEARCH ARTICLE
10.1029/2022WR034358

Key Points:
- A first conceptual and mathematical model is proposed to simulate the drift of victims of drowning in urban rivers
- Global sensitivity analysis reveals that knowing the body characteristics (mass, height) is critical to limit model outcome uncertainties
- The relative importance of other controlling parameters depends on the considered time horizon

Supporting Information:
Supporting Information may be found in the online version of this article.

Correspondence to:
C. Delhez,
clement.delhez@uliege.be

Citation:
Delhez, C., Rivière, N., Erpicum, S., Pirotton, M., Archambeau, P., Arnst, M., et al. (2023). Drift of a drowning victim in rivers: Conceptualization and global sensitivity analysis under idealized flow conditions. *Water Resources Research*, *59*, e2022WR034358. https://doi.org/10.1029/2022WR034358

Received 9 JAN 2023
Accepted 22 SEP 2023

Author Contributions:
Conceptualization: C. Delhez
Data curation: C. Delhez
Formal analysis: C. Delhez, B. Dewals
Investigation: C. Delhez
Methodology: C. Delhez, M. Arnst
Resources: C. Delhez, B. Dewals
Software: C. Delhez
Supervision: N. Rivière, B. Dewals
Validation: C. Delhez
Visualization: N. Rivière, S. Erpicum, M. Pirotton, P. Archambeau, B. Dewals
Writing – original draft: C. Delhez
Writing – review & editing: C. Delhez, N. Rivière, S. Erpicum, M. Arnst, J. Bierens, B. Dewals

Drift of a Drowning Victim in Rivers: Conceptualization and Global Sensitivity Analysis Under Idealized Flow Conditions

C. Delhez[1], N. Rivière[2], S. Erpicum[1], M. Pirotton[1], P. Archambeau[1], M. Arnst[3], J. Bierens[4], and B. Dewals[1]

[1]Hydraulics in Environmental and Civil Engineering (HECE), Research Unit Urban & Environmental Engineering (UEE), University of Liège, Liège, Belgium, [2]Univ Lyon, INSA Lyon, Ecole Centrale de Lyon, Université Claude Bernard Lyon I, CNRS, LMFA, UMR 5509, Villeurbanne, France, [3]Aerospace and Mechanical Engineering, University of Liège, Liège, Belgium, [4]VU University Medical Centre, Amsterdam, The Netherlands

Abstract We present a conceptual model of the drift of a drowning victim in a river, accounting for the mechanical effects of body decomposition. The model was tested under idealized flow conditions (uniform flow) and a global sensitivity analysis was performed. Uncertainties in body morphology, flow-body interaction parameters (e.g., drag coefficient) and drowning characteristics were considered. The results emphasize the importance of predicting the body vertical position since it considerably influences the streamwise body drift velocity, due to the significant difference between near-surface and near-bed velocity. The results also highlight the value of testimonies providing information on body mass and height, as decreasing uncertainty on these input data strongly reduces uncertainties on the predicted body streamwise position. Next step of the research will consist in coupling the model with an Eulerian multi-dimensional model of river hydrodynamics.

1. Introduction

1.1. Context

Worldwide, unintentional drowning is estimated to cause about 400,000 fatalities every year (WHO, 2014). Climate change tends to increase the risk of drowning, due to a rising frequency and magnitude of hydro-meteorological extremes (Musolino et al., 2020). More frequent riverine and flash floods increase the likelihood of persons being drifted by watercourses (Chen et al., 2019; Lazzarin et al., 2022; Milanesi et al., 2015; Musolino et al., 2020). Repeated heatwaves (Simpkins, 2017) lead to a rise in (unauthorized) bathing activities in urban rivers and a corresponding rise in drowning accidents.

Understanding the trajectory of human bodies drifted in streams is of great interest for informing targeted rescue operations and for reducing the resources needed for body search and recovery after drowning. A short reaction time is key for rescue missions. Depending on water temperature, resuscitation may be possible in a time window of up to one and a half hour after drowning (Tipton & Golden, 2011). A quick, target-oriented, and process-informed search can make the difference between finding the victim alive or dead. Even beyond this time frame, a speedy recovery of the human body remains important. It enables search and rescue teams to act quicker, improve resources allocation, and it reduces the risks taken by first-responders such as divers. Body search operations in urban rivers are dangerous and complex due to relatively high flow velocity and momentum combined with a low visibility due to suspended materials and dissolved compounds (Horn, 2014). Search technologies such as sonars typically perform poorly in urban river stretches due the presence of various debris and man-made artifacts on the river bottom (Blondel, 2014). During floods, high flow momentum and transported debris (stones, tree trunks, vehicles …) make it unsafe for search and rescue staff to boat or dive, so that locating a victim of drowning during flood becomes hardly possible (Ray, 2014).

After drowning and loss of consciousness, three stages of vertical body motion may typically be distinguished (Bierens, 2015; Heaton et al., 2010; Mateus et al., 2013). First, the body sinks and reaches the bed as its overall density is generally slightly above that of fresh water. Water inhalation and ingestion also plays a role in this motion since it leads to replacing air in the human body by water and, therefore, it alters the body bulk density. Second, body entrainment takes place on the riverbed. It is influenced by fluid forces, bed friction, bed morphology, gravity, and buoyancy as well as body positioning and deformability. Third, putrefaction gases are generated after a period of time (typically two to 5 days) which depends on water temperature. The gases increase

10.1029/2022WR034358

the buoyancy and, unless the body is entangled at the river bed, it eventually resurfaces and drifts (Lunetta et al., 2014). The exact duration of each of the three stages remains complex to predict as it depends on several factors such as body characteristics, clothing, flow conditions, and water temperature.

1.2. State of the Art

So far, studies in forensic medicine focused on aspects such as characterizing the cause of drowning (Stephenson et al., 2020) or estimating of the post-mortem submersion interval (PMSI) for bodies retrieved from water (Heaton et al., 2010; Mateus et al., 2013; Papadodima et al., 2010; van Daalen et al., 2017). The PMSI is generally estimated as the time elapsed between the suspected moment of the drowning accident and the moment when an eyewitness noticed the body at the water surface. PMSI may be used as a proxy for the time elapsed until body resurfacing, despite a risk of overestimation of the resurfacing time. The values of PMSI reported in literature vary considerably from one case study to another (e.g., 12–192 days according to Heaton et al. (2010)). This is due to the influence of temperature on body decomposition (Hayman & Oxenham, 2016; Kaatsch et al., 1994; Megyesi et al., 2005), which is not encompassed in the PMSI.

Therefore, other studies in forensic medicine introduced the concept of accumulated degree day (ADD) as defined by Megyesi et al. (2005). The ADD is evaluated as the integral over time of the temperature of the environment in which the body is situated (e.g., water temperature):

$$\mathrm{ADD} = \int_{t_0}^{t} T\,dt \qquad (1)$$

where t_0 stands for the initial time of the drowning, t is the current time and T is the environment temperature. Empirical data suggest that ADD is a reasonable predictor to estimate the degree of decomposition of a dead body (Heaton et al., 2010; van Daalen et al., 2017) and, therefore, the resurfacing time (Megyesi et al., 2005). Indeed, the values of ADD corresponding to observed resurfacing time of bodies of victims were found to vary in a narrower range than the corresponding PMSI (Megyesi et al., 2005).

So far, search operations in urban rivers have not been guided by any modeling technique aiming at predicting the trajectory of the victim's body. Existing computational studies of body drift trajectories were developed for marine environments (Breivik & Allen, 2008; Carniel et al., 2002; Gunduz, 2017; Hart-Davis & Backeberg, 2023; Ličer et al., 2020; Mateus et al., 2015; Tu et al., 2021; Wu et al., 2023) and, as such, they focused on the effects of wind, waves, and currents. In most cases, the vertical body motion was neglected (Carniel et al., 2002). This assumption was justified by the relatively higher density of saltwater compared to freshwater, so that the body has a greater chance of floating (Carniel et al., 2002; Ebbesmeyer & Haglund, 1994; Mateus et al., 2015). Life jackets are also more commonly used in marine environments than in the case of drowning accidents in rivers. For inland water bodies, the vertical body motion needs to be considered to enable reliable predictions of body streamwise position (Heaton et al., 2010), hence body decomposition has a considerable influence.

In existing models developed for marine environments, the grid size varies between 1 and 9 km (Breivik & Allen, 2008; Carniel et al., 2002; Gunduz, 2017; Hart-Davis & Backeberg, 2023; Ličer et al., 2020; Mateus et al., 2015). This is two to three orders of magnitude coarser than the mesh refinement necessary to capture the typical topographic variability of most urban rivers worldwide. The length scale characterizing the body of a victim of drowning remaining unchanged (∼2 m) irrespective of the drowning context, the two problems appear fundamentally different between river and sea/ocean contexts. Indeed, in marine environments, the body being drifted has a characteristic size way smaller than the length scales characterizing the forcings (flow and wind fields), whereas in rivers they are less separated or even comparable (flow structures such as secondary currents or vertical velocity gradients both developing across the river depth, thus with a O(1–10 m) characteristic length, large vortices downstream bridge piers with a O(1 m) characteristic length, etc.). Now, the interaction between body being drifted and flow is strongly controlled by the ratio of body scale to flow scale (Ghaffarian et al., 2020; Meninno et al., 2020). The time scales are also significantly different. Existing modeling studies in marine environments use time steps between 1 and 12 hr, while a time step suitable for resolving the trajectory of a body in the flow field of an urban river needs to be considerably smaller. Overall, the sea/ocean context enables a separation of scale between the forcings and the drifted body, whereas this does not apply to the context of urban rivers, hence making the coupling between flow and body drift more intricate in the case of rivers since more fine-scale

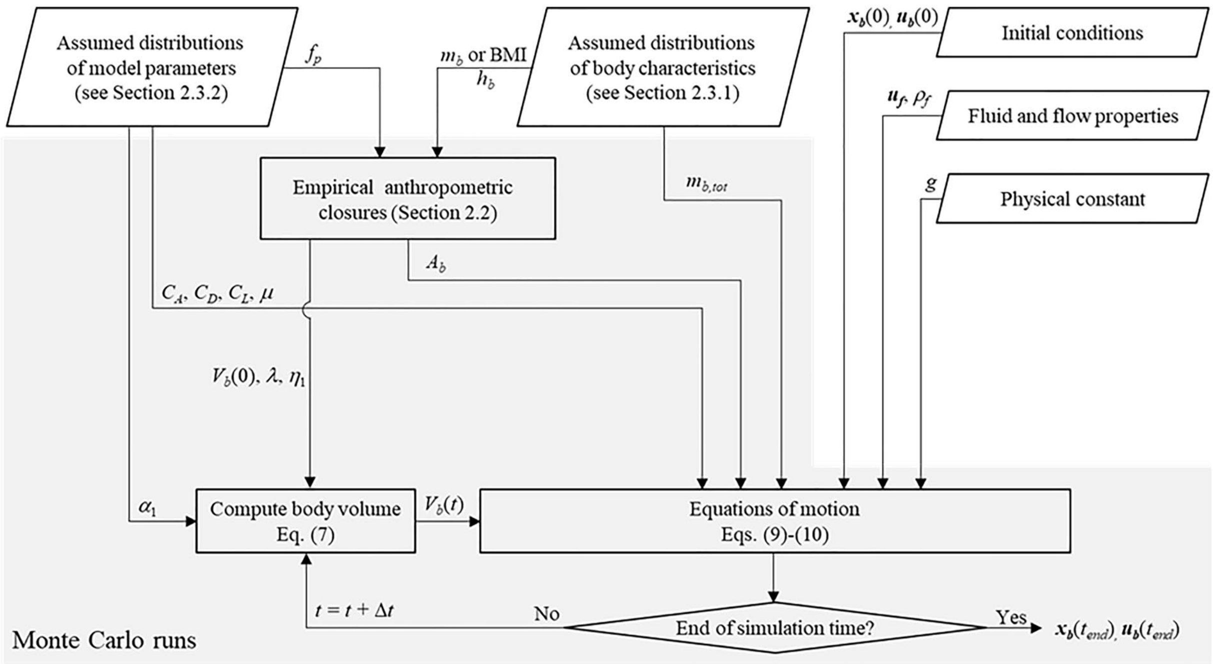

Figure 1. Workflow of the modeling.

aspects need to be resolved. In one recent computational study (Gonzalez et al., 2022), flow fields in rivers were calculated to identify areas (e.g., vortices) where a body is likely to remain trapped, but the drift of an individual body was not reproduced explicitly.

1.3. Objective

In the present study, we propose a new conceptual and mathematical formulation for describing the drift of the body of a drowning victim in rivers considering the mechanical effects of body decomposition. We first formulate the model in general terms, and then it is analyzed for idealized flow conditions (uniform flow). Under this assumption, the body trajectory is computed in two dimensions: along the streamwise direction and over the flow depth. The flow velocity is assumed to vary over the flow depth following a logarithmic profile. The body drift model is Lagrangian. It is based on force balance coupled with a new, original equation for predicting the evolution of the body volume (hence, also, body bulk density) as a function of elapsed time and water temperature (through ADD). This makes the model able to predict the three observed stages of body vertical displacement: sinking, bloating and resurfacing. A global sensitivity analysis is presented to inform on the relative influence of uncertainties in input data and model parameters on model outcomes. Results show a strong correlation between body streamwise motion and vertical positioning of the body over the flow depth.

2. Methodology

This study presents a Lagrangian drift model based on a balance of forces acting on a human body. A general model formulation is first introduced. It is subsequently analyzed considering idealized, uniform flow conditions. The modeling strategy involves two components. First, a mechanistic model solves the equations of motion based on a set of input data and model parameters, as well as a new hypothesis on the evolution of body characteristics (volume, bulk density) as a result of body decomposition (Section 2.1). Empirical anthropometric closures are used to infer the necessary geometric and physical characteristics of the body from a limited number of inputs, such as estimated body mass or body mass index (BMI; Section 2.2). Second, this mechanistic model is embedded within a stochastic modeling framework (Section 2.3), in which a Monte Carlo approach is adopted to account for uncertainties in the input data and model parameters and assess the sensitivity of model outcomes to these uncertainties. The workflow of the modeling is sketched in Figure 1, while more details are given in

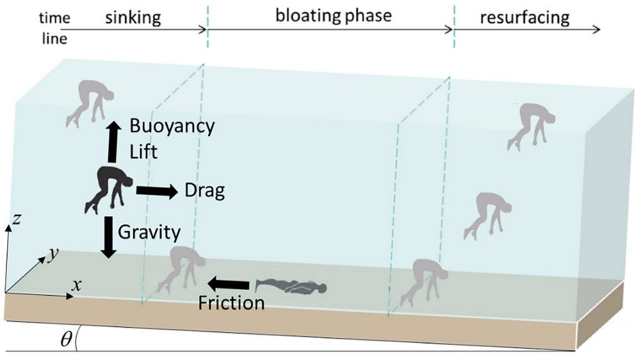

Figure 2. Conceptualization of sinking, bloating, and resurfacing phases (adapted from Mateus et al. (2013)).

Figure S1 in Supporting Information S1. The new methodology was applied to several scenarios of flow conditions and body characteristics, as defined in Section 2.4.

2.1. Mechanistic Model

2.1.1. Governing Equations

The body trajectory is described based on the position and velocity of its center of mass. Neither the body orientation (roll, pitch, and yaw angles) nor possible posture deformations are explicitly predicted by the model. Instead, we consider variations in body orientation and deformation via statistical distributions characterizing the body frontal area, body drag coefficient, or friction coefficient on the riverbed, among others (Section 2.3).

A Cartesian reference frame is used, where the x-axis is aligned with the mean slope of the river bed, as shown in Figure 2. The independent variables are time t and the vector of spatial coordinates $\boldsymbol{x} = [x, y, z]^{\mathrm{T}}$. The angle between the x-axis and the horizontal plane is denoted θ. The flow field is steady and is assumed to be given as input data, that is, the flow depth $h(\boldsymbol{x}, t)$ and the flow velocity $\boldsymbol{u_f}(\boldsymbol{x}, t) = [u_f, v_f, w_f]^{\mathrm{T}}$ are considered to be known. The bed level $b(x, y)$ is known also.

In the Lagrangian drift model, the state variables are the body position vector $\boldsymbol{x_b} = [x_b, y_b, z_b]^{\mathrm{T}}$ and its associated velocity vector $\boldsymbol{u_b} = [u_b, v_b, w_b]^{\mathrm{T}}$. The model equations write:

$$\dot{\boldsymbol{x}}_{\boldsymbol{b}} = \boldsymbol{u_b} \tag{2}$$

$$\left(m_{b,\mathrm{tot}}\mathbf{I} + \frac{1}{2}\mathbf{C_A}\rho_f V_{b,\mathrm{sub}}\right)\dot{\boldsymbol{u}}_{\boldsymbol{b}} = \boldsymbol{F_f} + \boldsymbol{F_g} + \boldsymbol{F_b}, \tag{3}$$

where a dot over a variable refers to the time derivative, $m_{b,\mathrm{tot}}$ is the total body mass, $\mathbf{C_A}$ the second-order tensor of added mass coefficients, ρ_f the fluid density, $V_{b,\mathrm{sub}}$ the submerged body volume, $\boldsymbol{F_f}$ the fluid to body forces (drag, side, and lift), $\boldsymbol{F_g}$ the resultant of gravity and buoyancy forces, and $\boldsymbol{F_b}$ the friction force on the bottom. The body is assumed unconscious, so that swimming efforts do not need to be considered in the force balance. The "total body mass" differs from the initial body mass by the amount dm of water swallowed and aspirated at the time of drowning: $m_{b,\mathrm{tot}} = m_b + dm$. The body volume evolves with time, as detailed in Section 2.1.2.

In general, the variation range of the dependent variables x_b and y_b is constrained by the width of the water course and the presence of rigid obstacles (e.g., bridge piers, abutments). Similarly, the elevation z_b of the body center of mass varies between a minimum value, equal to $b(x_b, y_b) + \varepsilon_{\min}$, and a maximum value, which is close to the free surface elevation. The length $\varepsilon_{\min}$ is a body characteristic, representing roughly the body "thickness."

The fluid to body force may be expressed as follows, Equation 4:

$$\boldsymbol{F_f} = -\frac{1}{2}\rho_f \mathbf{C}\left(\boldsymbol{u_b} - \boldsymbol{u_f}\right)|\boldsymbol{u_b} - \boldsymbol{u_f}|, \tag{4}$$

where $\mathbf{C}$ is a second-order tensor whose elements are products of drag, lift and side coefficients by the respective frontal areas. The balance of gravity and buoyancy forces reads:

$$\boldsymbol{F_g} = \mathbf{g}(m_{b,\mathrm{tot}} - \rho_f V_{b,\mathrm{sub}}), \tag{5}$$

where $\mathbf{g}$ is the gravity acceleration vector $[g \sin\theta, 0, -g\cos\theta]^{\mathrm{T}}$.

For the friction force between the body and the bottom, a parametrization based on Coulomb formulation is proposed:

$$\begin{cases} \boldsymbol{F_b} = -\mu\,\gamma(\boldsymbol{x_b})\,g\cos\theta\,\max(m_{b,\mathrm{tot}} - \rho_f V_{b,\mathrm{sub}}, 0)\,\frac{1}{\sqrt{u_b^2+v_b^2}}\begin{bmatrix} u_b \\ v_b \\ 0 \end{bmatrix} & \text{if } u_b^2 + v_b^2 \neq 0 \\ \boldsymbol{F_b} = \mathbf{0} & \text{if } u_b^2 + v_b^2 = 0 \end{cases}, \tag{6}$$

10.1029/2022WR034358

where μ is a Coulomb-type friction coefficient and $\gamma(\boldsymbol{x_b})$ is a continuous "shape" function ensuring that $\boldsymbol{F_b}$ becomes non-negligible only when the body is positioned close to the bottom (Figure S2 in Supporting Information S1). The exact formulation used for function $\gamma(\boldsymbol{x_b})$ is inspired from the standard Rouse profile for suspended sediments (Rouse, 1950), see Equation S1 in Supporting Information S1.

2.1.2. Mechanical Effects of Body Decomposition

The submerged body volume $V_{b,\mathrm{sub}}$, which intervenes in Equations 3, 5 and 6, varies with time due to two effects: the generation of putrefaction gases in the body as body decomposition progresses, and the depth-dependent water pressure acting on the body external surface. We consider that the body volume is composed of two parts: (a) a fixed part which corresponds to the volume occupied by solid material such as bones and flesh, and (b) a variable part which corresponds to the volume occupied by gas within the body. The former is supposed time-independent while the latter evolves with time. The portion of the total volume occupied by gas, λ, was approximated here as the lungs volume, and estimated by means of empirical closures as detailed in Section 2.2 and in Supporting Information S1.

To conceptualize the mechanical effects of body decomposition, we hypothesize that the variable part of the body volume changes under the influence of two competing drivers: the water pressure p_{hydro} acting on the body and the degree of body decomposition η (varying between 0, i.e., no effect of decomposition on body volume, and η_1 a maximum value reached when the body tissues refrain further body expansion or putrefaction ceases). This leads to the following model formulation for the body volume as a function of time:

$$V_b(t) = (1-\lambda)\, V_b(0) + \lambda\, V_b(0)\,(1+\eta)\left(1 - \frac{p_{\mathrm{hydro}}}{E}\right)^3 \tag{7}$$

with $V_b(0)$ the volume of the body prior to drowning and E the Young modulus of the rib cage. The value of E for the rib cage was estimated at 11.7 MPa (Vezin & Verriest, 2007; Youssef, 2012). The last factor in the right-hand-side of Equation 7 represents the contraction of the rib cage under the effect of water pressure, while factor $(1+\eta)$ reflects the body expansion due to decomposition.

As highlighted in Section 1, the degree of body decomposition may be predicted based on the ADD, as defined in Equation 1 and noted α hereafter. Putrefaction is the dominating decomposition process which influences body volume. The kinetics of putrefaction involves a gradual start, followed by a rapid increase and a stabilization (Bierens, 2015). For these reasons, we propose to link α and the rate η of increase in body volume due to decomposition (Figure S3 in Supporting Information S1):

$$\eta\left(\frac{\alpha}{\alpha_1}\right) = \eta_1\ \min\left[6\left(\frac{\alpha}{\alpha_1}\right)^5 - 15\left(\frac{\alpha}{\alpha_1}\right)^4 + 10\left(\frac{\alpha}{\alpha_1}\right)^3 ; 1\right] \tag{8}$$

with α_1 the value of ADD reached when the body cannot expand further due to tissues resistance or fading of putrefaction processes.

2.1.3. Uniform Flow

In the case of uniform (i.e., steady and fully-developed) flow conditions, the flow field is given by $\boldsymbol{u_f} = [u_f(z), 0, 0]^{\mathrm{T}}$, the flow depth h is constant and, in the frame of reference introduced in Figure 2, the bottom elevation b is considered equal to 0 everywhere. Under these conditions, Equations 2 and 3 can be written as:

$$\begin{bmatrix} \dot{x}_b \\ \dot{z}_b \end{bmatrix} = \begin{bmatrix} u_b \\ w_b \end{bmatrix} \tag{9}$$

$$\begin{aligned}\left(m_{b,\mathrm{tot}} + \frac{1}{2} C_A \rho_f V_b\right)\begin{bmatrix} \dot{u}_b \\ \dot{w}_b \end{bmatrix} = &-\frac{1}{2}\rho_f A_b \begin{bmatrix} C_D \\ C_L \end{bmatrix}(u_b - u_f)|u_b - u_f| + g(m_{b,\mathrm{tot}} - \rho_f V_{b,\mathrm{sub}})\begin{bmatrix} \sin\theta \\ -\cos\theta \end{bmatrix} \\ &- \mathrm{sign}(u_b)\mu\,\gamma(z_b)\, g\cos\theta\ \max(m_{b,\mathrm{tot}} - \rho_f V_{b,\mathrm{sub}}, 0)\begin{bmatrix} 1 \\ 0 \end{bmatrix}\end{aligned} \tag{10}$$

10.1029/2022WR034358

where the effect of added mass was assumed isotropic: $\mathbf{C_A} = C_A\,\mathbf{I}$, with C_A the added mass coefficient. Forces induced by the relative velocity between body and flow along direction z were neglected. This has little influence on the results due to the short duration of the vertical displacements.

For the sake of simplicity, $u_f(z)$ was supposed to follow a logarithmic profile over the flow depth (Figure S4 in Supporting Information S1):

$$u_f(z) = \frac{\overline{u}_f}{\frac{z_0}{h} - 1 + \ln\frac{h}{z_0}} \ln\frac{z}{z_0} \tag{11}$$

with $\overline{u}_f$ the depth-averaged flow velocity, and z_0 the depth at which the flow velocity reaches zero. Parameter z_0 depends on the roughness height k_s and the flow regime (Pope, 2000). To prevent Equation 11 from predicting negative flow velocities, parameter $\varepsilon_{\min}$ was set to a value greater than z_0.

The ordinary differential equations Equations 9 and 10 were discretized using an explicit Euler scheme. To improve computational efficiency, a variable time step was considered. It varies between 0.01 s in regions where the body experiences substantial acceleration (e.g., during sinking, when approaching the bottom, at the time of resurfacing), and takes values up to 60 s when the body is essentially moving at a constant velocity (e.g., during bloating on the riverbed, or when drifted at the water surface after resurfacing).

2.2. Empirical Anthropometric Relations

Existing empirical equations were used to provide an estimate of body characteristics required by the model, such as the frontal area A_f, the initial body volume $V_b(0)$, the portion λ of gas in the body volume, and the maximum rate of body expansion η_1. They apply for adult subjects.

2.2.1. Frontal Area, A_f

The frontal area of a body depends on the body morphology, posture and orientation with respect to the flow direction. Here, we assumed that the body positioning matches the typical positioning of an unconscious person floating in water, that is, body facing the bottom with the limbs hanging down (Lunetta et al., 2014) as sketched in Figure 2.

For given values of the body mass and height, the body frontal area was estimated in two steps, as detailed in Section C1 in Supporting Information S1. First, the body surface area (BSA) was computed using empirical equations proposed by Tikuisis et al. (2001) which is formula among others (Du Bois & Du Bois, 1989; Mosteller, 1987). Second, the frontal area was derived from the BSA by means of an empirical projection coefficient f_p whose value is estimated to range between 0.16 and 0.36 (Tanabe et al., 2000). The uncertainties arising from the difficulty of setting a clear-cut value for f_p was considered in our sensitivity analysis (Section 2.3).

2.2.2. Initial Body Volume, $V_b(0)$

The initial body volume $V_b(0)$ was approximated as the body volume at functional residual capacity (FRC) of the lungs. Empirical relations proposed by Liu et al. (2017) and Sendroy and Collison (1965) were used to estimate the body volume at FRC as a function of the body mass, height and BMI. These relations are detailed in Section C2 in Supporting Information S1.

2.2.3. Functional Residual Capacity

As the body volume at lungs FRC was taken as a proxy for the initial body volume $V_b(0)$, the lungs volume at FRC was also estimated to provide a first approximation for parameter λ in Equation 7. The lungs volume at FRC is known to vary between approximately 1.7 and 3.5 L depending on body gender, age, height, and BMI, among other parameters (Abston et al., 2017; Miller, 2005; Stocks & Quanjer, 1995). As detailed in Section C3 in Supporting Information S1, we combined empirical results of Stocks and Quanjer (1995) and Abston et al. (2017) to determine the FRC from the gender, age, body height and BMI.

2.2.4. Total Lungs Capacity

The total lungs capacity (TLC) may vary between 3.4 and 9.0 L depending on the gender, body height, BMI, etc. (Abston et al., 2017; Miller, 2005; Stocks & Quanjer, 1995). In line with the approximation used for FRC,

10.1029/2022WR034358

we combined equations proposed by Stocks and Quanjer (1995) and Abston et al. (2017) to estimate the lungs volume from the gender, body height and BMI, as described in Section C4 in Supporting Information S1. A first approximate value for η_1 was evaluated by assuming that the maximum increase in the body volume may be appreciated by considering the difference between the TLC and the FRC. This aspect certainly needs to be refined in further research.

2.3. Stochastic Framework

To account for the substantial uncertainties affecting the input data and model parameters (e.g., body height, mass, kinetics of body decomposition, etc.), the model presented in Section 2.1 was run in a stochastic framework using a Monte Carlo approach (Metropolis & Ulam, 1949). The uncertainty affecting each uncertain input data and model parameter was described based on statistical distributions. The considered distributions were either directly derived from observations, or theoretical distributions were adjusted to match observations. Depending on the uncertain variable, a uniform distribution (e.g., Goeury et al. (2022)), or a beta distribution was used. Beta distributions involve two parameters (α and β), as detailed in Section D in Supporting Information S1 and described in McDonald and Xu (1995). Table 1 summarizes the main characteristics of the statistical distributions selected for each input data and model parameter, as detailed in Sections 2.3.1 and 2.3.2. Next, total order Sobol' indices were computed to quantify the sensitivity of model outcomes (i.e., body position at time t) to uncertain data and parameters (Section 2.3.3).

2.3.1. Input Data

For the body height and mass (or BMI), two scenarios were considered: either it is assumed that no specific information is available on the body characteristics (e.g., absence of eyewitness), or the body characteristics are relatively well known (e.g., description by a relative of the victim).

- In the first case (Scenario "unknown body"), a beta distribution was adjusted to reflect the variety of body heights and BMI over the whole Belgium population, as reported by Van Der Heyden et al. (2018). Distinct distributions were used for female and for male victims (Figure S5 in Supporting Information S1). The BMI was considered for the estimation of body mass. This enables accounting for existing correlations between body height and mass. As displayed in Figure S6 in Supporting Information S1, a beta distribution was adjusted for BMI to fit data also made available by Van Der Heyden et al. (2018).
- In the second case (Scenario "known body"), the body height was assumed to follow a beta distribution in which the 10th and 90th percentiles correspond to the mode of the distribution ±2.5 cm (Figure S7 in Supporting Information S1). Similarly, the body mass was described by a beta distribution in which the 10th and 90th percentiles correspond to the mode of the distribution ±2.5 kg (Figure S8 in Supporting Information S1). The distribution ranges were selected to reflect the remaining uncertainties in body characteristics even when this information is reported by relatives of the victim or by eye-witnesses of the drowning accident (Meissner et al., 2007).

Modell and Davis (1969) measured the amount of water inside the lungs of 74 victims of drowning in freshwater. The measurements revealed that 14% of the victims had aspirated more than 22 g of water per kg of body weight. Accordingly, we adjusted here a beta distribution for the ratio dm/m_b, ensuring that percentile 86 of the distribution corresponds to 22 g/kg.

2.3.2. Model Parameters

Delhez et al. (2021) conducted flume experiments to estimate the drag coefficient of a human body. They considered reduced-scale dummies, positioned like the typical posture observed for real-world drowning victims, that is, face down and limbs hanging down (Section 2.1). The empirical distribution of observed drag coefficients is shown in Figure S9 in Supporting Information S1.

To the best of the authors' knowledge, no experimental data exist for the value of the lift coefficient of a human body in a typical drowning position nor in similar postures. Data are mostly available for simple shapes, such as for instance a spherical body, for which C_L is close to 0.5 Legendre and Magnaudet (1998). To be on the safe side, it was assumed that the uncertainty in the value of the lift coefficient may be described by a uniform distribution over the range [0; 1].

The added mass coefficient C_A depends on the shape of the considered object. According to Newman and Grue (2017), C_A equals unity for circular cylinders, as used by Ghaffarian et al. (2020) and Persi et al. (2018), and

10.1029/2022WR034358

Table 1
Considered Distributions of Uncertain Inputs and Parameters for Adult Subjects

	Variable	Symbol	Source	Observations	Distribution	Range	Parameters
Input data	Body height (scenario "unknown body")	h_b	Van Der Heyden et al. (2018)	p_{25}, p_{50}, p_{75}, and average	Beta	[1.5; 2.05] m (male)	$\alpha = 5.8697$, $\beta = 6.075$ (male)
						[1.4; 1.9] m (female)	$\alpha = 3.976$, $\beta = 5.965$ (female)
	BMI (scenario "unknown body")	BMI	Van Der Heyden et al. (2018)	p_{25}, p_{50}, p_{75}, and average	Beta	[15; 40] kg/m^2	$\alpha = 3.0102$, $\beta = 4.2628$
	Body height ("known body")	h_b	What if scenario	Assumed mode, p_{10} and p_{90}	Beta	[1.5; 2.05] m	$\alpha = 116.8$, $\beta = 66.65$
	Body mass ("known body")	m_b	What if scenario	Assumed mode, p_{10} and p_{90}	Beta	[40; 150] kg	$\alpha = 200$, $\beta = 467$
	Swallowed water	dm/m_b	Modell and Davis (1969)	p_{86}	Beta	[0; 0.026]	$\alpha = 1.5$ and $\beta = 1.25$
Model parameters	Drag coefficient	C_D	Laboratory experiments	Lab data (Figure S9 in Supporting Information S1)	Empirical	–	–
	Lift coefficient	C_L	Legendre and Magnaudet (1998)	C_L for a sphere for similar Re	Uniform	[0; 1]	–
	Added mass coefficient	C_A	Newman and Grue (2017)	Values for a cylinder and for a sphere	Uniform	[0.25; 1]	–
	Projection coefficient	f_p	Tanabe et al. (2000)	Range	Uniform	[0.16; 0.36]	–
	ADD threshold value	$\alpha_1/2$	Mateus et al. (2013)	Range	Beta	[95; 117]	$\alpha = \beta = 1.8024$
	Friction coefficient	μ	Keller and Mitsch (1993) and Jonkman and Penning-Rowsell (2008)	Range	Uniform	[0.3; 1]	–

Note. Notations p_{25}, p_{50}, and p_{75} refer to the percentiles 25, 50, and 75.

$C_A = 0.5$ for a sphere. Based on experiments conducted with human subjects, Caspersen et al. (2010) found that C_A for swimmers can be as low as 0.25. We considered this value as a lower bound for our analyses. Given the substantial differences between the typical drowning position and that of swimmers [see photograph below], and the possible effects of clothes or accessories (e.g., backpack), we considered here values of C_A ranging between 0.25 and 1 (i.e., value applicable for a cylinder). The distribution of C_A was assumed uniform in this range. Considering a relatively wide range of possible values for C_A is on the safe side, and the outcomes of the present study enable appreciating whether getting a better knowledge of C_A in the case of drowning would be valuable for the modeling, or whether the model results are hardly sensitive to the value of C_A.

For the projection factor f_p used to estimate the frontal area (Section C1 in Supporting Information S1), we assumed a uniform distribution over the range [0.16; 0.36], which corresponds to the range of values measured by Tanabe et al. (2000) for seated or standing bodies. Values characterizing standing bodies can be transposed to lying ones as these two positions are equivalent from the perspective of hydrodynamic coefficients provided that the pitch angle is shifted by 90°.

In Equation 8 describing the kinetics of body decomposition, the value $\alpha_1/2$ may be regarded as similar to the threshold value of ADD above which the body resurfaces (Heaton et al., 2010; Mateus et al., 2013; Megyesi et al., 2005). Based on field observations, Mateus et al. (2013) report threshold values for ADD between 95 and 117°C days. Therefore, as shown in Figure S10 in Supporting Information S1, we considered here a beta distribution for parameter $\alpha_1/2$ with parameters $\alpha = \beta = 1.8024$ over the range [95; 117].

For the coefficient μ characterizing the friction between a body and the riverbed, a uniform distribution was assumed over the range [0.3; 1], in line with ranges reported by Keller and Mitsch (1993) and Jonkman and Penning-Rowsell (2008).

2.3.3. Variance-Based Sensitivity Analysis

To quantify the sensitivity of the model outcomes to the uncertainties in input data and model parameters, we computed total order Sobol' indices (Sobol, 2001) either for individual uncertain variables (Section 3.2) or for groups of them (Section 3.3). In line with Arnst and Ponthot (2014), we proceeded in three steps:

- first, 20,000 runs of the model introduced in Section 2.1 were performed based on a reference sample generated by randomly assigning values to the uncertain variables listed in Table 1, according to their respective statistical distributions;
- next, to compute the Sobol' index associated to one specific (group of) uncertain variable(s), another series of 20,000 model runs (modified sample) was conducted, in which only the value(s) of the considered (group of) uncertain variable(s) was changed, while all other variables were kept at the same value as in the reference sample;
- the corresponding Sobol' index s_x was calculated as follows:

$$S_x = \frac{\frac{1}{2n}\sum_{i=1}^{n}\left(x_{b,ref,i} - x_{b,mod,i}\right)^2}{Var(x_b)} \quad (12)$$

with n the size of the sample and x_b the body streamwise position at the considered time. Subscript *ref* refers to the reference sample, and subscript *mod* the modified sample.

The number of 20,000 runs was selected based on a convergence analysis of the model. As shown in Section E in Supporting Information S1, the necessary number of runs to reach convergence depends on the considered parameter and type of body (e.g., gender). In the case of Sobol' index computation for parameter BMI in the scenario UB-HF (women), almost 10,000 runs are needed to reach convergence (Figure S11 in Supporting Information S1). Therefore, we opted for a sample size of 20,000, composed of the same number of men and women.

2.4. Test Program

Two flow scenarios and two types of body samples were considered in the analyses presented in Section 3.

A "high flow" (rapid) and a "low flow" (slow) scenario were tested. In the former case, the depth-averaged flow velocity was set to 0.12 m/s, while in the latter case it was taken equal to 3 m/s. Assuming a constant flow depth

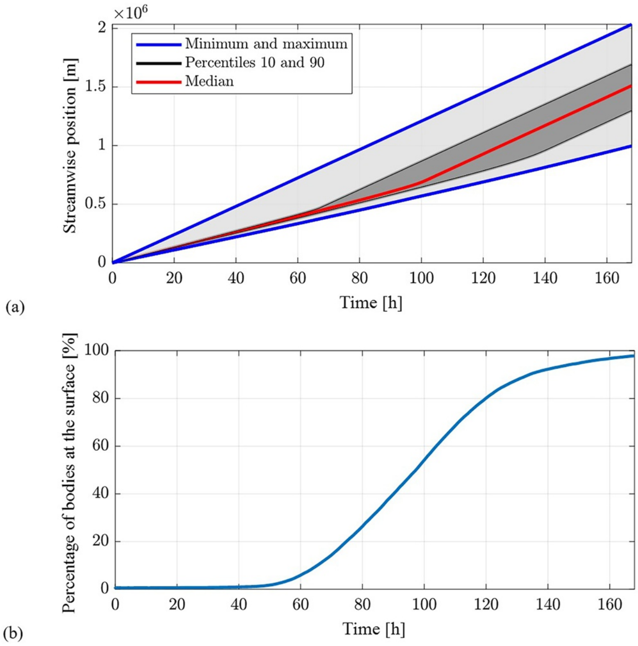

Figure 3. (a) Streamwise positions of bodies as a function of time in scenario "unknown" body in high flow scenario. (b) Percentage of bodies at the surface.

of 6 m, this corresponds to Froude numbers of 0.016 and 0.39, respectively. These values cover a plausible range for typical Froude numbers in lowland urban rivers. Using the body height as a characteristic length (Ungerechts & Hollander, 1982), the corresponding Reynolds numbers are respectively of the order of 2×10^5 and 6×10^6 for the high and the low flow scenarios. Note that the assumed value of water depth has limited influence on the modeling results. This is mainly due to the very short duration of vertical motions (sinking or resurfacing) compared to other characteristic times.

As detailed in Section 2.3, the sample of bodies was assumed either completely unknown (e.g., no eyewitness testimony nor indications obtained from relatives), in which case the distributions of body characteristics extend over a wide range, or the body was considered as relatively well known, with body characteristics spanning over narrower ranges. The body considered in this scenario is a body of 1.85 m and 73 kg irrespective of the gender.

Combining the two flow scenarios and the two types of body samples leads to four scenarios, with an "unknown" body in low flow scenario (UB-LF), "unknown" body in high flow scenario (UB-HF), "known" body in low flow scenario (KB-LF) and "known" body in high flow scenario (KB-HF).

The water density was assumed equal to 1,000 kg/m³ and its temperature equal to 24°C. This value is realistic for summer conditions in some large urban rivers. Moreover, the choice of this value of water temperature has little influence on the conducted analyses. Indeed, water temperature is only involved in the estimation of ADD (Equation 1 in Section 1.2), which is used here to linearly scale the time. Hence, in our study, assuming a smaller water temperature would only linearly shrink the horizontal axes of graphs displaying model results as a function of ADD (such as in Figure 4 hereafter).

Parameter z_0 in Equation 11 was set equal to 1.3 mm, while parameter ε_{min} was set to 0.2 m. The presented computational results are based on 20,000 Monte Carlo runs, in which men and women are equally represented. This number was enough to ensure convergence of the results analyzed here (Section E in Supporting Information S1).

3. Results and Discussion

The results are presented and discussed in two steps. First, an overview of the modeling results is presented through the evolution of the body streamwise position and its standard deviation (Section 3.1). The latter is an indicator of practical relevance as it reflects the extent over which search operations should be targeted. Second, the outcomes of the global sensitivity analyses are introduced, both for individual parameters (Section 3.2) and for groups of parameters (Section 3.3).

3.1. Body Streamwise Position

3.1.1. Model Outcomes

The developed model predicts the evolution of body streamwise position and its relative positioning over the flow depth. In most Monte Carlo runs, the computed body trajectory involves sinking after a relatively short period (2 min ±1 min), followed by bloating and finally resurfacing. The time elapsed until body resurfacing varies considerably: its median value is 95 hr, with a standard deviation of 16 hr. In a limited number of runs (about 2%), the computed trajectory remains at the water surface (no sinking). This occurs when the randomly selected combination of body characteristics (mass or BMI, heights …) leads to buoyancy exceeding the body submerged weight. Conversely, in few runs (less than 1%), the model predicts body sinking and bloating but no resurfacing. Again, this results from a randomly selected combination of parameter values (deemed plausible) which led to buoyancy remaining insufficient to trigger resurfacing despite the effects of body decomposition.

Figure 3a displays statistics of body streamwise position as a function of time for scenario UB-HF. Similar figures related to the other scenarios are provided in Section F in Supporting Information S1. The line corresponding to

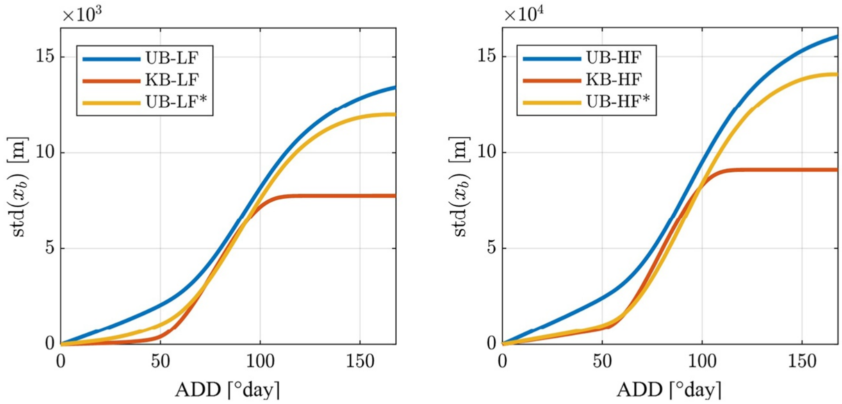

Figure 4. Standard deviation of the streamwise position of the bodies as a function of accumulated degree day (ADD).

the median streamwise position shows a change in slope close to $t = 95$ hr, which matches the median resurfacing time. The change of slope reflects contrasting body drift velocities depending on whether the body is close to the riverbed (no drift in low flow scenarios, and drift velocity of the order of 2 m/s in high flow scenarios) or near the free surface (drift velocity of the order of 0.1 and 3 m/s in low and high flow scenarios, respectively). This considerable difference in drift velocity explains the observed rise in the dispersion of the body streamwise positions (see the interdecile range) when an increasing number of model runs predicts body resurfacing (Figure 3b). In Figure 3a, the lines representing the minimum and maximum streamwise positions correspond, respectively, to model runs in which the body does not resurface and does not sink.

Figure 4 shows the evolution of the standard deviation of the body streamwise position as a function of ADD. Irrespective of the considered scenario, the standard deviation of the streamwise position follows the same pattern (Figure 4): a gradual increase (Stage 1), followed by a steeper increase (Stage 2), and eventually a milder increase and stabilization (Stage 3).

Scenarios UB-LF and UB-HF lead to the highest values of standard deviation over the whole duration of the simulations compared to KB-LF and KB-HF, respectively. Moreover, the standard deviation continues to grow even in Stage 3. In Stage 1, the values of standard deviation obtained for scenarios KB-LF and KB-HF are considerably lower than in the other two scenarios. This difference is reduced in Stage 2. In Stage 3, the computed standard deviations for scenarios KB-LF and KB-HF become independent of time. This contrasts with the results obtained for scenarios UB-LF and UB-HF. The overall behavior of the computed standard deviations does not change between the low and high flow scenarios, although the values are about 20% higher in the latter case. Figure 4 highlights that the availability of data on the body characteristics of the victim is instrumental to reduce the level of uncertainty on the body streamwise position. This suggests that collecting testimonies of eyewitnesses giving information on the victim's height and mass (or BMI) is of high value in practice.

Note that the distinctive results obtained here for Scenarios KB-LF and KB-HF, when compared to Scenarios UB, are related to the fact that the chosen body characteristics in these scenarios ensure that there are no bodies which do not sink nor do not resurface. If the particular case of non-sinking or non-resurfacing body was selected in Scenarios KB-LF or KB-HF, three possible outcomes are possible:

- if non-sinking bodies are considered, the standard deviation of the streamwise position becomes quickly a constant as all the bodies tend to travel at the same velocity as the surface flow; the distribution of body streamwise position is unimodal;
- if only non-resurfacing bodies are considered, the distribution of body streamwise position may be either unimodal or bimodal depending on the relative importance of friction and drag forces. The balance of these forces controls whether a body remains at rest or moves on the bottom. The distribution of body streamwise position is bimodal if some of the considered bodies remain at rest while others travel close to the bottom. The distribution is unimodal if, either all considered bodies remain at rest on the bottom, or all of them move close to the bottom.

3.1.2. Model Runs Without Uncommon Drowning Process

As emphasized in Figures 3b and 3% of the sample does not follow the standard sequence of sinking, bloating, and resurfacing. Alternate scenarios labeled UB-LF* and UB-HF* displayed in Figure 4 represents results obtained

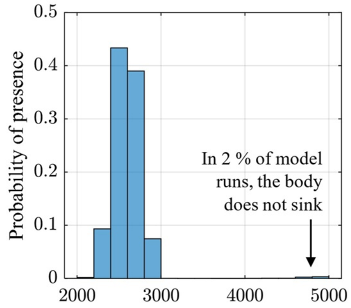

Figure 5. Distribution of body streamwise position computed for scenario "unknown" body in high flow scenario after 30 min.

with the same sample from which this 3% was removed. Note that this share of model runs is comparatively lower than the value of 7% mentioned by Donoghue and Minnigerode (1977), but it remains plausible. Indeed, unlike in Donoghue and Minnigerode (1977), we focus here on drowned bodies and we consider that water is swallowed and inhaled at the moment of drowning, which tends to reduce the buoyancy.

Relying on the previous analysis of KB scenarios, we hypothesize that the reason why the standard deviation of the streamwise position does not reach a constant value in Stage 3 (scenarios UB-LF and UB-HF in Figure 4) is precisely linked to these specific cases for which no sinking nor resurfacing of the body is computed, with the standard-deviation of UB scenarios keeping increasing due to the non-resurfacing bodies. Figure 5 also hints into this direction, as it reveals a bimodal distribution of the body streamwise position, with a few model runs predicting a significantly larger travel distance due to the absence of body sinking in these runs. For longer time horizons, a third mode in the distribution may also arise due to body trajectories involving sinking but no resurfacing.

Therefore, for scenarios UB-LF and UB-HF, the standard deviation of the body streamwise position was recomputed by discarding the cases in which the model did not predict body sinking nor resurfacing.

The results for scenarios UB-LF* and UB-HF* are the following: in Stage 1, the standard deviation remains relatively low; in Stage 2, it is lower than in scenarios UB-LF and UB-HF; and in Stage 3 the standard deviation becomes also independent of time like in scenarios KB-LF and KB-HF (although about 50° days later). This confirms that the absence of stabilization of the standard deviation in scenarios UB-LF and UB-HF is solely due to a small portion of model runs in which the model does not predict body sinking or resurfacing, combined with the considerable difference in drift velocity between bodies remaining at (or near) the surface, and those situated close to the riverbed. This is further analyzed in the next section.

3.1.3. Interpretation

Figure 6 shows the time derivative of the standard deviation of the body streamwise position as a function of the standard deviation of the relative elevation of the bodies in the flow depth. The latter quantity reflects the dispersion in body elevations in the various model runs, that is, the dispersion between "slowly-drifting" bodies located close to the bed and "fast-drifting" bodies positioned near the surface.

Figure 6 highlights that in every scenario the standard deviation of the streamwise position first rises at an increasing rate, as a rising number of model runs predict body resurfacing while some model runs still predict that the body remains close to the bed. Next, the rate of increase of the standard deviation of the body streamwise position becomes constant or nearly constant, as the dispersion in the vertical body positioning decreases. This is because virtually all model runs predict body resurfacing.

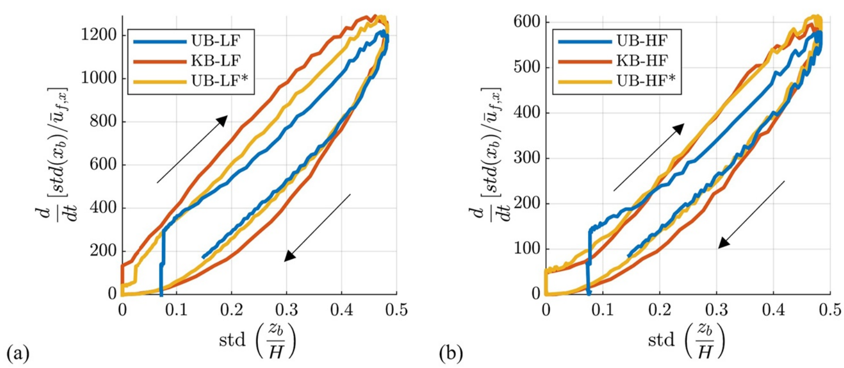

Figure 6. Time derivative of the standard deviation of the streamwise position of the bodies over average flow velocity in the streamwise direction as a function of the standard deviation of the vertical position over the water depth. (a) for low flow conditions and (b) for high flow conditions.

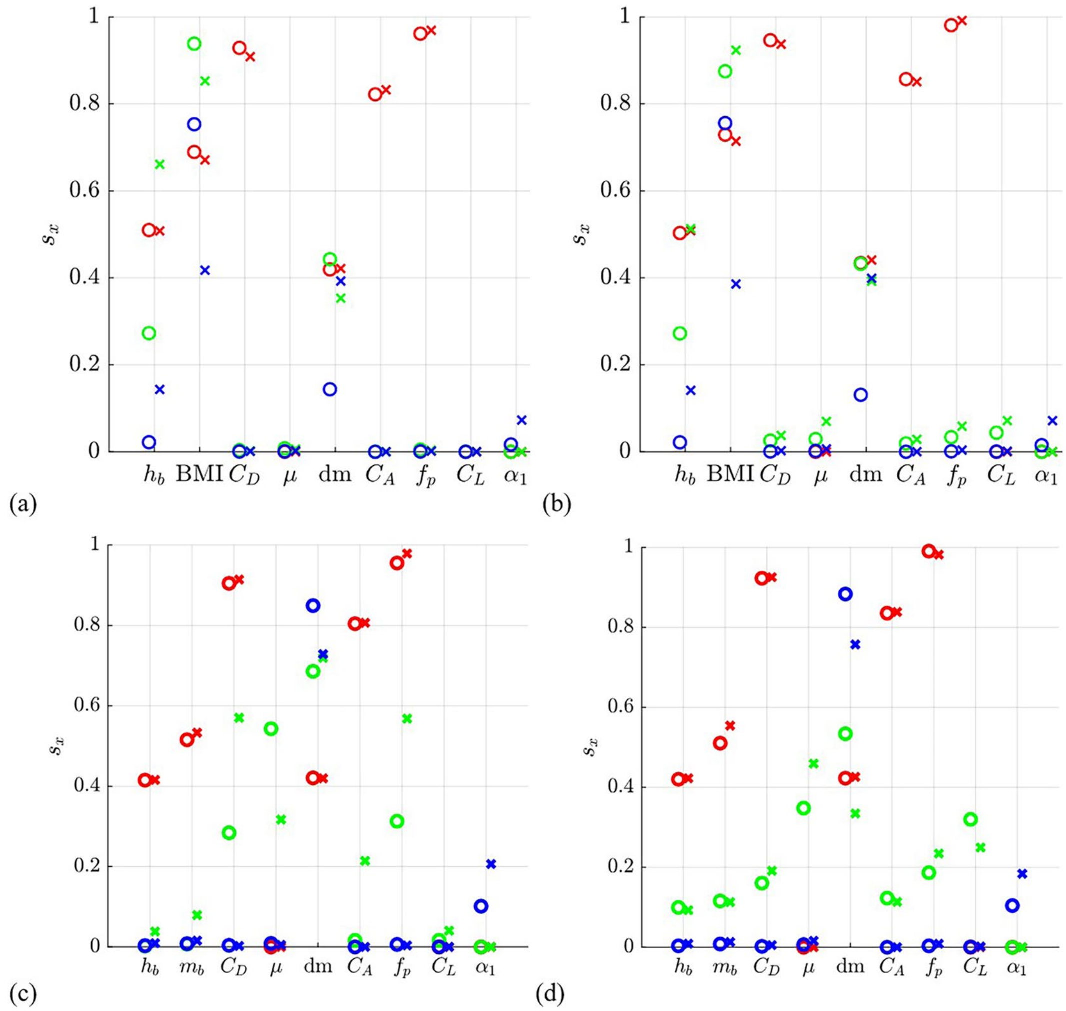

Figure 7. Sobol' indices for Scenarios (a) "unknown" body in low flow scenario, (b) "unknown" body in high flow scenario, (c) "known" body in low flow scenario, and (d) "known" body in high flow scenario. Red corresponds to the short time horizon ($t = 5$ min, without sinking), green to the intermediate time horizon ($t = 1$ hr, without resurfacing), and blue to the long time horizon ($t = 7$ days). Results for male bodies are represented by circles (○) and for female bodies by crosses (×).

In scenarios KB-LF and KB-HF, as well as UB-LF* and UB-HF*, the rate of change of the standard deviation of the body streamwise position ends up at zero, consistently with Figure 4. For scenarios UB-LF and UB-HF, neither the standard deviation of the vertical body position nor the rate of change of the standard deviation of the body streamwise position decline to zero, which is also in agreement with Figure 4.

From a practical perspective, this highlights that the uncertainty on the body streamwise position is strongly influenced by the uncertainty in its vertical position, and hence the need for reliably simulating the body decomposition process, which controls the body vertical motion.

3.2. Sobol' Indices for Individual Parameters

Sobol' indices were computed for scenarios UB-LF, UB-HF, KB-LF, and KB-HF (Figure 7) considering three different settings:

- over a short time horizon ($t = 5$ min) and assuming no sinking, that is, the components along z in Equations 9 and 10 are not solved and the body is assumed to remain at the surface,

- over an intermediate time horizon (t = 1 hr, i.e., typical duration after which initial search operations are stopped), accounting for sinking but not for body decomposition, that is, Equation 7 is not solved and, after sinking, the body is assumed to remain on the river bottom,
- over a longer time horizon (t = 7 days), accounting for sinking and body decomposition.

According to Figure 4, the 7-day time horizon is long enough to ensure that the standard deviation of the body streamwise position becomes independent of time in Scenarios KB-LF and KB-HF. In all cases, Sobol' indices were computed separately for men and women as uncertainty on body height and weight are gender dependent.

3.2.1. Short Time Horizon

Irrespective of the scenario and of the victim's gender, Figure 7 reveals that, over a short time horizon (t = 5 min), the most influential uncertainties arise from the projection factor, the drag coefficient C_D and the added mass coefficient C_A (Sobol' indices between 0.8 and 1). Uncertainties in the BMI and/or body mass, and body height, as well as the amount of swallowed water also have a substantial influence (Sobol' indices 0.4 and 0.8). This is consistent with the processes controlling the initial horizontal body acceleration, that is, the drag force and body inertia. The other potential sources of uncertainties (μ, C_L, and α_1) have no influence on the results since the vertical motion was not considered for this short time horizon.

3.2.2. Intermediate Time Horizon

For the intermediate time horizon (t = 1 hr), in which body decomposition and resurfacing are not considered, uncertainties in body height, BMI and amount of swallowed water have an overwhelming influence in the case of Scenarios UB-LF and UB-HF, with Sobol' indices close to 0.9 for BMI, of the order of 0.4 for dm and ranging between 0.3 and 0.7 for h_b. The value of Sobol' index related to all other model parameters remains below 0.1 (Figures 7a and 7b). In Scenario UB-LF, the value of the Sobol' indices for these other model parameters are even very close to zero (Figure 7a). This is because, after sinking, the simulated bodies tend to remain at rest on the bottom in the scenario involving low flow conditions (UB-LF), as can be seen in Figure S12 in Supporting Information S1, whereas they move on the bottom in the other scenario (UB-HF, Figure 3a).

In Scenarios KB-LF and KB-HF, a very small uncertainty is assigned to the input data (h_b and m_b) corresponding to those which show a dominating influence in Scenarios UB-LF and UB-HF, that is, h_b and m_b or BMI. This difference in the parameters uncertainty explains the smaller corresponding Sobol' indices obtained in the former cases. In Scenarios KB-LF and KB-HF, uncertainties in several parameters (μ, C_D, f_p, and C_A) have a strong influence on the model outcomes, while their effects were overshadowed in Scenarios UB-LF and UB-HF due to the assumed large uncertainties in h_b and BMI. The influence of uncertainty in the amount of swallowed water remains also large.

This can be interpreted as follows. In the KB-LF and KB-HF scenarios, the body height and mass vary little (Figures S13 and S14 in Supporting Information S1), so that variations in the body density remain also very limited. Hence, since the body density (close to 1,015 kg/m³ in our example) remains similar to the water density, small variations in other vertical forces such as the lift have a high chance to completely change the vertical equilibrium, and hence either induce or prevent sinking of the body. Similarly, due to the small buoyancy effect, slight changes in drag force (influenced by C_D and f_p) may trigger, prevent, or alter body motion on the bottom (even in the KB-LF Scenario). This is the reason why uncertainties in the friction coefficient have also a large influence on the results in this scenario.

3.2.3. Long Time Horizon

For Scenario UB-LF and UB-HF, over a long time horizon (t = 7 days), the uncertainties significantly influencing the body motion are those related to input data and model parameters ruling body resurfacing: BMI, body height, amount of swallowed water and the threshold value of ADD. In Scenarios KB-LF and KB-HF, the most influencing uncertainties remain the same except for body height and mass which become negligible. The differences in the results for female and male victims stem from the gender-dependent empirical closures used to estimate body volume (Section 2.2).

10.1029/2022WR034358

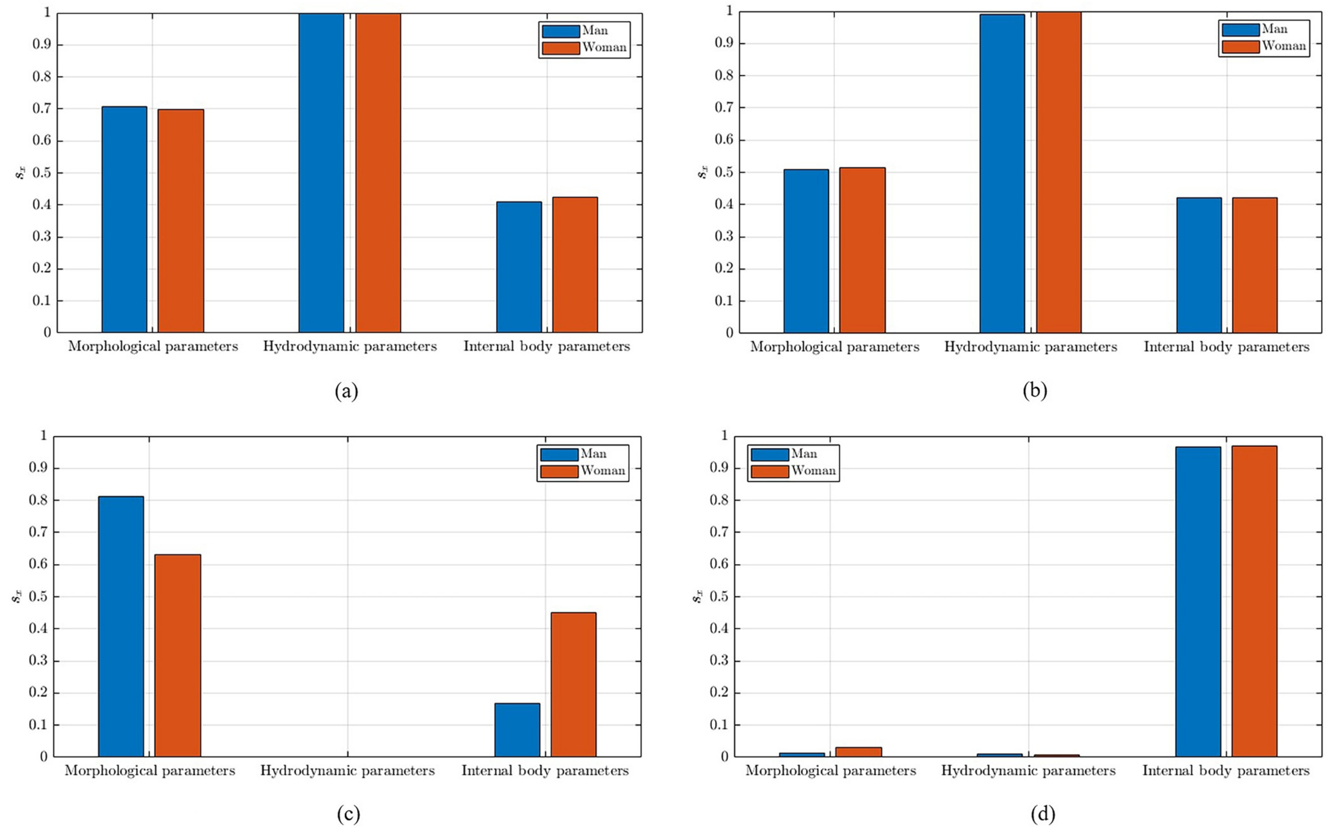

Figure 8. Sobol' index for groups of uncertain parameters. (a) Scenario "unknown" body in low flow scenario (UB-LF), $t = 5$ min. (b) Scenario "known" body in low flow scenario (KB-LF), $t = 5$ min. (c) Scenario UB-LF, $t = 7$ days. (d) Scenario KB-LF, $t = 7$ days.

3.3. Sobol' Indices for Groups of Parameters

As the interpretation of Sobol' indices evaluated for individual parameters remains intricate due to the number of uncertain parameters, we repeated the procedure for groups of parameters. The following three groups of parameters were considered:

- morphological parameters: h_b, and m_b or BMI
- hydrodynamic (flow-body interaction) parameters: C_D, C_A, C_L, and f_p
- internal body parameters: dm and α_1.

For the low flow scenario and a short time horizon ($t = 5$ min, without sinking), Figures 8a and 8b show that uncertainties in the hydrodynamic parameters are responsible for most of the variability in the body horizontal position. The morphological parameters also have an influence through the frontal area and the body inertia, while the internal body parameter dm influences the body inertia, hence its initial acceleration. In Scenario KB-LF, uncertainty in morphological parameters is small and it is responsible for limited variations in the body streamwise position. Nonetheless, since the overall variance of body positions over a short time horizon of 5 min is also limited, the Sobol' index still reveals a substantial contribution of these morphological parameters to the overall uncertainty.

Conversely, for the low flow scenario and a long time horizon ($t = 7$ days - Figures 8c and 8d), the most influential source of uncertainty in Scenario UB-LF is related to the morphological parameters, followed by those on the internal body parameters. The Sobol' indices related to the hydrodynamic parameters are close to zero irrespective of the gender. These results agree with those obtained for the Sobol' indices for individual parameters, and they appear sensible. Indeed, the morphological parameters (body height and BMI) have a direct influence on the body volume, and hence on both the buoyancy (controlling the sinking and resurfacing processes) as well as the Coulomb-type friction force (influenced by buoyancy). Conversely, the acceleration phases, controlled by the hydrodynamic parameters, are of particularly short duration compared to the time horizon considered here, so that the influence of the hydrodynamic parameters becomes negligible.

In contrast, in Scenario KB-LF, the sensitivity to the uncertainty in the morphological parameters is considerably reduced (Figure 8d), and only the internal body parameters show a significant influence since they control the resurfacing process.

Results for the intermediate time horizon ($t = 1$ hr, without resurfacing) as well as for the high flow scenarios can be found in Figures S15–S22 in Supporting Information S1.

4. Conclusion

Existing computational models aiming at predicting the drift of a victim of drowning were mostly developed for marine environments. As such, they do not reproduce the typical pattern followed by a body drowned in a river, that is, sinking, bloating and resurfacing. Computing the body position over the flow depth is instrumental for predicting the body streamwise position due to the considerable difference in drift velocity between a floating body and a body sliding or rolling on the riverbed. Empirical knowledge in forensic medicine indicates that the body bloating kinetics is controlled by both time and water temperature, and it can be related to the number of ADDs.

4.1. Key Findings

We propose here a first formulation of a mathematical model which enables reproducing this pattern. The newly introduced equation describes the evolution of the body volume under the competing influences of body decomposition and external hydrostatic pressure. This new component of the model relies on a limited number of parameters, which all have a physical interpretation: the initial void fraction in the body, a maximal body expansion rate, and a threshold value for ADD.

The model was analyzed in detail for idealized flow conditions corresponding to a uniform (i.e., steady and fully-developed) flow. Two flow scenarios were considered (low and high flow). Given the uncertainties affecting the knowledge of body characteristics and model parameters in real-world situations, a stochastic framework was adopted, in which statistical distributions were assumed for the uncertain input data and model parameters. It led to the following findings:

- In the tested cases, the variance of the computed body streamwise positions is reduced by a factor of the order of two if precise information (height, mass) is available on the characteristics of the victim. This highlights the critical importance of testimonies by eyewitnesses of the accidents or by relatives of the victim.
- The computed distribution of body streamwise position is generally multimodal, with one mode corresponding to model runs in which the body does not sink, the main one related to the standard pattern of sinking, bloating and resurfacing, and in rare cases a third mode corresponding to model runs in which the body does not resurface.
- By means of global sensitivity analysis, we highlighted the relative importance of each source of uncertainty. For a short time horizon, that is, prior to body sinking, the parameters controlling the estimation of drag force and body inertia are the most influential ones since the dominating process during this phase is body acceleration to reach the flow velocity. For longer time horizons, uncertainties in parameters ruling the evolution of body density tend to be very influential since they directly affect the occurrence of sinking and/or resurfacing as well as the Coulomb-type friction force on the riverbed.
- When the body characteristics are assumed highly uncertain, the impact of their uncertainty overwhelm most other sources of uncertainties. This points again at the importance of collecting high-quality information on the victim (e.g., through testimonies).

4.2. Remaining Challenges

Remaining scientific challenges are numerous. In priority, the model needs to be extended to more general flow settings. The proposed Lagrangian model may be coupled with flow field information irrespective of how the flow field data was generated (e.g., 1D, 2D, or 3D Eulerian modeling). However, specific challenges remain to be addressed, such as modeling the interaction between a drifting body and riverbanks, bridge piers or other obstacles. Whether common river hydrodynamic models provide a sufficient resolution of the flow field at specific locations, such as in the wake of a bridge pier, needs to be investigated. Such questions were partly addressed for the drift of logs in rivers (Persi et al., 2018; Ruiz-Villanueva et al., 2014); but the methods need to be transferred to the case of the drift of a human body. If a 2D Eulerian hydrodynamic model is used, questions arise regarding the parametrization of complex velocity profile over the flow depth in the near-field of structures such as bridge piers, abutments, or weirs …

The influence of turbulence should be considered more explicitly in the model. In the current mathematical formulation, effects of turbulence are only implicitly embedded in the assumed distribution of flow velocity over the depth, as expressed by Equation 3. However, the randomness arising from turbulence is not yet reflected in the drift model. This may lead to underestimations of the variability in body location. Several options exist to account for the turbulence-induced randomness in body trajectories, such as adding stochastic perturbations to the body position, velocity, or acceleration. These approaches are referred to as "Markov models" of varying order (Berloff & McWilliams, 2002; Reijnders et al., 2022). Previous studies of human body drift in oceans have focused only on random walk approaches (e.g., Carniel et al., 2002). A different approach was used by Ruiz-Villanueva et al. (2014) for simulating the transport of tree logs in turbulent open-channel flow. They added stochastic fluctuations not to the object velocity but to the flow velocity used in the Lagrangian momentum equation. These fluctuations could be calculated from the turbulence model used in the Eulerian flow computation (e.g., k-ε model) and a random number. We recommend transposing this approach to the case of human body drift in rivers. In this way, identical bodies dropped at the same spot would follow various trajectories, which would differ more if the flow turbulence intensity is higher.

There is also room for improvement in the Lagrangian drift model itself. So far, neither the body orientation (roll, pitch, and yaw angles) nor possible posture deformations are explicitly predicted by the model. Also, the model does not account for existing correlations between parameters such as drag or added mass coefficients and the body characteristics (height, mass). The same applies for correlations between the victim's age and body density (Durnin & Womersley, 1974), or the influence of clothing. Tackling these challenges requires more transdisciplinary research involving expertise in forensic medicine, river hydrodynamics, uncertainty quantification as well as experimental techniques for conducting laboratory and field observations (e.g., using carefully designed dummies able to mimic the behavior of a human body).

Validation of the presented model against field data will be a cornerstone of further model development and its establishment as a tool to guide rescue and search operations in urban rivers. Gathering the necessary data and developing the framework for model validation also requires interdisciplinary and intersectoral collaborations with forensic medicine, first responders (police, fireplace brigade, and civil safety), water authorities and courts.

Although additional practical challenges need to be overcome, related to computational efficiency and data assimilation, among other aspects, this research paves the way for more effective planning of rescue and, above all, search operations for the sake of reducing risks taken by first responders and reducing the time of body retrieval.

Data Availability Statement

Data and software were not used, nor created for this research.

Acknowledgments

The first author gratefully acknowledges a fellowship received through a grant *Fonds Spéciaux pour la Recherche* (FSR) of the School of Engineering of the University of Liege. The authors thank to Dr. Philipp Selzer for his valuable feedback on an early version of the manuscript.

References

Abston, E., Comellas, A., Reed, R. M., Kim, V., Wise, R. A., Brower, R., et al. (2017). Higher BMI is associated with higher expiratory airflow normalised for lung volume (FEF25–75/FVC) in COPD. *BMJ Open Respiratory Research*, *4*(1), e000231. https://doi.org/10.1136/bmjresp-2017-000231

Arnst, M., & Ponthot, J.-P. (2014). An overview of nonintrusive characterization, propagation, and sensitivity of uncertainties in computational mechanics. *International Journal for Uncertainty Quantification*, *4*(5), 387–421. https://doi.org/10.1615/int.j.uncertaintyquantification.2014006990

Berloff, P. S., & McWilliams, J. C. (2002). Material transport in oceanic gyres. Part II: Hierarchy of stochastic models. *Journal of Physical Oceanography*, *32*(3), 797–830. https://doi.org/10.1175/1520-0485(2002)032<0797:mtiogp>2.0.co;2

Bierens, J. J. L. M. (2015). *Drowning: Prevention, rescue, treatment* (2nd ed. 2014 éd.). Springer-Verlag Berlin and Heidelberg GmbH & Co. K.

Blondel, P. (2014). Searching for dead bodies with sonar. In J. Bierens (Ed.), *Drowning*. Springer. https://doi.org/10.1007/978-3-642-04253-9_182

Breivik, Ø., & Allen, A. A. (2008). An operational search and rescue model for the Norwegian Sea and the North Sea. *Journal of Marine Systems*, *69*(1–2), 99–113. https://doi.org/10.1016/j.jmarsys.2007.02.010

Carniel, S., Umgiesser, G., Sclavo, M., Kantha, L. H., & Monti, S. (2002). Tracking the drift of a human body in the coastal ocean using numerical prediction models of the oceanic, atmospheric and wave conditions. *Science & Justice: Journal of the Forensic Science Society*, *42*(3), 143–151. https://doi.org/10.1016/s1355-0306(02)71819-4

Caspersen, C., Berthelsen, P. A., Eik, M., Pâkozdi, C., & Kjendlie, P. L. (2010). Added mass in human swimmers: Age and gender differences. *Journal of Biomechanics*, *43*(12), 2369–2373. Epub 2010 May 23. PMID: 20546755. https://doi.org/10.1016/j.jbiomech.2010.04.022

Chen, Q., Xia, J., Falconer, R. A., & Guo, P. (2019). Further improvement in a criterion for human stability in floodwaters. *Journal of Flood Risk Management*, *12*(3), e12486. https://doi.org/10.1111/jfr3.12486

Delhez, C., Erpicum, S., & Dewals, B. (2021). *Hydrodynamic characterisation of a body-like shape: A contribution to guide the search for victims of drowning in rivers*. IAHR.

Donoghue, E. R., & Minnigerode, S. C. (1977). Human body buoyancy: A study of 98 men. *Journal of Forensic Sciences*, *22*(3), 573–579. https://doi.org/10.1520/jfs10628j

Du Bois, D., & Du Bois, E. F. (1989). A formula to estimate the approximate surface area if height and weight be known. 1916. *Nutrition*, *5*, 303–311. Discussion 312–313.

Durnin, J. V. G. A., & Womersley, J. (1974). Body fat assessed from total body density and its estimation from skinfold thickness: Measurements on 481 men and women aged from 16 to 72 years. *British Journal of Nutrition*, *32*(01), 77–97. https://doi.org/10.1079/bjn19740060

Ebbesmeyer, C. C., & Haglund, W. D. (1994). Drift trajectories of a floating human body simulated in a hydraulic model of Puget Sound. *Journal of Forensic Sciences*, *39*(1), 231–240. https://doi.org/10.1520/jfs13590j

Ghaffarian, H., Lopez, D., Mignot, E., Piegay, H., & Riviere, N. (2020). Dynamics of floating objects at high particulate Reynolds numbers. *Physical Review Fluids*, *5*, 054307. https://doi.org/10.1103/physrevfluids.5.054307

Goeury, C., Bacchi, V., Zaoui, F., Bacchi, S., Pavan, S., & El kadi Abderrezzak, K. (2022). Uncertainty assessment of flood hazard due to levee breaching. *Water*, *14*(23), 3815. https://doi.org/10.3390/w14233815

Gonzalez, J. R. P., Escobar-Vargas, J., Vargas-Luna, A., Castiblanco, S., Trujillo, D., Guatame, A. C., et al. (2022). Hydroinformatics tools and their potential in the search for missing persons in rivers. *Forensic Science International*, *341*, 111478. https://doi.org/10.1016/j.forsciint.2022.111478

Gunduz, M. (2017). Possible recovery site of four non-recovered bodies lost in the Marmara Sea by using an ocean circulation model. *Australian Journal of Forensic Sciences*, *49*(2), 154–160. https://doi.org/10.1080/00450618.2016.1138320

Hart-Davis, M. G., & Backeberg, B. C. (2023). Towards a particle trajectory modelling approach in support of South African search and rescue operations at sea. *Journal of Operational Oceanography*, *16*(2), 131–139. https://doi.org/10.1080/1755876x.2021.1911485

Hayman, J., & Oxenham, M. (2016). Supravital reactions in the estimation of the time since death (TSD). In J. Hayman & M. Oxenham (Eds.), *Human body DECOMPOSITION* (pp. 1–12). Elsevier.

Heaton, V., Lagden, A., Moffatt, C., & Simmons, T. (2010). Predicting the postmortem submersion interval for human remains recovered from U.K. Waterways. *Journal of Forensic Sciences*, *55*(2), 302–307. https://doi.org/10.1111/j.1556-4029.2009.01291.x

Horn, K. (2014). Underwater search and evidence response teams. In J. Bierens (Ed.), *Drowning* (pp. 1175–1177). Springer.

Jonkman, S. N., & Penning-Rowsell, E. (2008). Human instability in flood flows. *JAWRA Journal of the American Water Resources Association*, *44*(5), 1208–1218. https://doi.org/10.1111/j.1752-1688.2008.00217.x

Kaatsch, H.-J., Schmidtke, E., & Nietsch, W. (1994). Photometric measurement of pressure-induced blanching of livor mortis as an aid to estimating time of death: Application of a new system for quantifying pressure-induced blanching in lividity. *International Journal of Legal Medicine*, *106*(4), 209–214. https://doi.org/10.1007/bf01371339

Keller, R. J., & Mitsch, B. (1993). *Safety aspects of the design of roadways as floodways, research report/urban water research association of Australia*. Published for the Urban Water Research Association of Australia. The Melbourne Water Corporation.

Lazzarin, T., Viero, D. P., Molinari, D., Ballio, F., & Defina, A. (2022). A new framework for flood damage assessment considering the within-event time evolution of hazard, exposure, and vulnerability. *Journal of Hydrology*, *615*, 128687. https://doi.org/10.1016/j.jhydrol.2022.128687

Legendre, D., & Magnaudet, J. (1998). The lift force on a spherical bubble in a viscous linear shear flow. *Journal of Fluid Mechanics*, *368*, 81–126. https://doi.org/10.1017/s0022112098001621

Ličer, M., Estival, S., Reyes-Suarez, C., Deponte, D., & Fettich, A. (2020). Lagrangian modelling of a person lost at sea during the Adriatic scirocco storm of 29 October 2018. *Natural Hazards and Earth System Sciences*, *20*(8), 2335–2349. https://doi.org/10.5194/nhess-20-2335-2020

Liu, X., Niu, J., Ran, L., & Liu, T. (2017). Estimation of human body volume (BV) from anthropometric measurements based on three-dimensional (3D) scan technique. *Aesthetic Plastic Surgery*, *41*(4), 971–978. https://doi.org/10.1007/s00266-017-0872-5

Lunetta, P., Ebbesmeyer, C., & Molenaar, J. (2014). Behaviour of dead bodies in water. In J. Bierens (Ed.), *Drowning* (pp. 1149–1152). Springer.

Mateus, M., de Pablo, H., & Vaz, N. (2013). An investigation on body displacement after two drowning accidents. *Forensic Science International*, *229*(1–3), 6–12. https://doi.org/10.1016/j.forsciint.2013.03.010

Mateus, M., Pinto, L., & Chambel-Leitão, P. (2015). Evaluating the predictive skills of ocean circulation models in tracking the drift of a human body: A case study. *Australian Journal of Forensic Sciences*, *47*(3), 322–331. https://doi.org/10.1080/00450618.2014.957346

McDonald, J. B., & Xu, Y. J. (1995). A generalization of the beta distribution with applications. *Journal of Econometrics*, *66*(1–2), 133–152. https://doi.org/10.1016/0304-4076(94)01612-4

Megyesi, M. S., Nawrocki, S. P., & Haskell, N. H. (2005). Using accumulated degree-days to estimate the postmortem interval from decomposed human remains. *Journal of Forensic Sciences*, *50*(3), 618–626. https://doi.org/10.1520/jfs2004017

Meissner, C., Sporer, S., & Schooler, J. (2007). Person description as eyewitness evidence. In J. D. Read & M. P. Toglia (Eds.), *Handbook eyewitness psychology: Memory people* (pp. 3–34). Lawrence Earlbaum & Associates.

Meninno, S., Persi, E., Petaccia, G., Sibilla, S., & Armanini, A. (2020). An experimental and theoretical analysis of floating wood diffusion coefficients. *Environmental Fluid Mechanics*, *20*(3), 593–617. https://doi.org/10.1007/s10652-019-09693-x

Metropolis, N., & Ulam, S. (1949). The Monte Carlo method. *Journal of the American Statistical Association*, *44*(247), 335–341. https://doi.org/10.1080/01621459.1949.10483310

Milanesi, L., Pilotti, M., & Ranzi, R. (2015). A conceptual model of people's vulnerability to floods. *Water Resources Research*, *51*(1), 182–197. https://doi.org/10.1002/2014wr016172

Miller, M. R. (2005). Standardisation of spirometry. *European Respiratory Journal*, *26*(2), 319–338. https://doi.org/10.1183/09031936.05.00034805

Modell, J. H., & Davis, J. H. (1969). Electrolyte changes in human drowning victims. *Anesthesiology*, *30*(4), 414–420. https://doi.org/10.1097/00000542-196904000-00011

Mosteller, R. D. (1987). Simplified calculation of body-surface area. *New England Journal of Medicine*, *317*, 1098.

Musolino, G., Ahmadian, R., Xia, J., & Falconer, R. A. (2020). Mapping the danger to life in flash flood events adopting a mechanics based methodology and planning evacuation routes. *Journal of Flood Risk Management*, *13*(4), e12627. https://doi.org/10.1111/jfr3.12627

Newman, J. N., & Grue, J. (2017). *Marine hydrodynamics* (40th anniversary ed.). The MIT Press.

Papadodima, S. A., Athanaselis, S. A., Skliros, E., & Spiliopoulou, C. A. (2010). Forensic investigation of submersion deaths. *International Journal of Clinical Practice*, *64*(1), 75–83. https://doi.org/10.1111/j.1742-1241.2008.01890.x

Persi, E., Petaccia, G., & Sibilla, S. (2018). Large wood transport modelling by a coupled Eulerian–Lagrangian approach. *Natural Hazards*, *91*, 59–74. https://doi.org/10.1007/s11069-017-2891-6

Pope, S. B. (2000). *Turbulent flows* (1st ed.). Cambridge University Press.

Ray, S. (2014). Training and equipping rescue personnel for flood rescue. In J. J. L. M. Bierens (Ed.), *Drowning prevention, rescue, treatment* (pp. 491–494). Springer.

Reijnders, D., Deleersnijder, E., & Van Sebille, E. (2022). Simulating Lagrangian subgrid-scale dispersion on Neutral surfaces in the ocean. *Journal of Advances in Modeling Earth Systems*, *14*(2), e2021MS002850. https://doi.org/10.1029/2021ms002850

Rouse, H. (1950). *Engineering hydraulics*. John Wiley & Sons.

Ruiz-Villanueva, V., Bladé, E., Sánchez-Juny, M., Marti-Cardona, B., Díez-Herrero, A., & Bodoque, J. M. (2014). Two-dimensional numerical modeling of wood transport. *Journal of Hydroinformatics*, *16*(5), 1077–1096. https://doi.org/10.2166/hydro.2014.026

Sendroy, J., & Collison, H. A. (1965). *Determination of human body volume from height and weight*. Naval Medical Research Institute.

Simpkins, G. (2017). Increasing river flood risk. *Nature Climate Change*, *7*(3), 172. https://doi.org/10.1038/nclimate3243

Sobol, I. M. (2001). Global sensitivity indices for nonlinear mathematical models and their Monte Carlo estimates. *Mathematics and Computers in Simulation, The Second IMACS Seminar on Monte Carlo Methods*, *55*(1–3), 271–280. https://doi.org/10.1016/s0378-4754(00)00270-6

Stephenson, L., Stockham, P., van den Heuvel, C., & Byard, R. W. (2020). Characteristics of drowning deaths in an inner city river. *Legal Medicine*, *47*, 101783. https://doi.org/10.1016/j.legalmed.2020.101783

Stocks, J., & Quanjer, P. H. (1995). Reference values for residual volume, functional residual capacity and total lung capacity. ATS Workshop on Lung Volume Measurements. Official Statement of the European Respiratory Society. *European Respiratory Journal*, *8*(3), 492–506. https://doi.org/10.1183/09031936.95.08030492

Tanabe, S., Narita, C., Ozeki, Y., & Konishi, M. (2000). Effective radiation area of human body calculated by a numerical simulation. *Energy and Buildings*, *32*(2), 205–215. https://doi.org/10.1016/s0378-7788(00)00045-1

Tikuisis, P., Meunier, P., & Jubenville, C. (2001). Human body surface area: Measurement and prediction using three dimensional body scans. *European Journal of Applied Physiology*, *85*(3–4), 264–271. https://doi.org/10.1007/s004210100484

Tipton, M. J., & Golden, F. S. C. (2011). A proposed decision-making guide for the search, rescue and resuscitation of submersion (head under) victims based on expert opinion. *Resuscitation*, *82*(7), 819–824. https://doi.org/10.1016/j.resuscitation.2011.02.021

Tu, H., Wang, X., Mu, L., & Xia, K. (2021). Predicting drift characteristics of persons-in-the-water in the South China Sea. *Ocean Engineering*, *242*, 110134. https://doi.org/10.1016/j.oceaneng.2021.110134

Ungerechts, B. E., & Hollander, A. P. (1982). *Biomechanics and medicine in swimming* (pp. 215–221). Human Kinetics.

van Daalen, M. A., de Kat, D. S., Oude Grotebevelsborg, B. F. L., de Leeuwe, R., Warnaar, J., Oostra, R. J., & M Duijst-Heesters, W. L. J. (2017). An aquatic decomposition scoring method to potentially predict the postmortem submersion interval of bodies recovered from the North Sea. *Journal of Forensic Sciences*, *62*(2), 369–373. https://doi.org/10.1111/1556-4029.13258

Van Der Heyden, J., Nguyen, D., Renard, F., Scohy, A., Demarest, S., Drieskens, S., & Gisle, L. (2018). *Enquête de santé par examen belge*. Sciensano.

Vezin, P., & Verriest, J.-P. (2007). Vezin-1 development of a set of numerical human models for safety.

WHO. (2014). Global report on drowning: Preventing a leading killer.

Wu, J., Cheng, L., & Chu, S. (2023). Modeling the leeway drift characteristics of persons-in-water at a sea-area scale in the seas of China. *Ocean Engineering*, *270*, 113444. https://doi.org/10.1016/j.oceaneng.2022.113444

Youssef, M. (2012). *Analyse de l'influence des paramètres structuraux et fonctionnels d'une cage thoracique sous chargement dynamique a l'aide d'un modèle simplifiè*. Ingènierie biomèdicale. Universitè de Lyon.